PROCEEDINGS OF SPIE

Field effect photoconductivity in graphene on undoped semiconductor substrates

B. K. Sarker, E. Cazalas, I. Childres, T.-F. Chung, I. Jovanovic, et al.

SPIE.

Field Effect Photoconductivity in Graphene on Undoped Semiconductor Substrates

B. K. Sarker[a], E. Cazalas[b], I. Childres[a], T.F. Chung[a], I. Jovanovic[b,c], and Y. P. Chen*[a,d]

[a]Department of Physics and Astronomy, Birck Nanotechnology Center, Purdue University, West Lafayette, IN USA 47907; [b]Department of Mechanical and Nuclear Engineering, The Pennsylvania State University, University Park, PA USA 16802; [c]Department of Nuclear Engineering and Radiological Sciences, University of Michigan, Ann Arbor, MI USA 48109; [d]School of Electrical and Computer Engineering, Purdue Quantum Center, Purdue University, West Lafayette, IN USA 47907

*Email: yongchen@purdue.edu

ABSTRACT

Due to its high charge carrier mobility, broadband light absorption, and ultrafast carrier dynamics, graphene is a promising material for the development of high-performance photodetectors. Graphene-based photodetectors have been demonstrated to date using monolayer graphene operating in conjunction with either metals or semiconductors. Most graphene devices are fabricated on doped Si substrates with SiO_2 dielectric used for back gating. Here, we demonstrate photodetection in graphene field effect phototransistors fabricated on undoped semiconductor (SiC) substrates. The photodetection mechanism relies on the high sensitivity of the graphene conductivity to the local change in the electric field that can result from the photo-excited charge carriers produced in the back-gated semiconductor substrate. We also modeled the device and simulated its operation using the finite element method to validate the existence of the field-induced photoresponse mechanism and study its properties. Our graphene phototransistor possesses a room-temperature photoresponsivity as high as ~7.4 A/W, which is higher than the required photoresponsivity (1 A/W) in most practical applications. The light power-dependent photocurrent and photoresponsivity can be tuned by the source-drain bias voltage and back-gate voltage. Graphene phototransistors based on this simple and generic architecture can be fabricated by depositing graphene on a variety of undoped substrates, and are attractive for many applications in which photodetection or radiation detection is sought.

Keywords: Photodetectors, phototransistor, graphene, graphene field effect transistor, photoresponse, optoelectronics

1. INTRODUCTION

Graphene, a single layer of carbon atoms in a honeycomb lattice, is a fascinating new material with a potential for use in a variety of applications, including the next-generation electronic and optoelectronic devices.[1-5] In particular, graphene-based photodetectors have attracted significant attention due to their relatively wide absorption spectrum, high carrier mobility, low cost, and feasibility of their integration into flexible and transparent devices.[6-14] Over the last several years, a variety of graphene-based photodetectors have been reported.[6-24] Among these, significant efforts have been devoted to developing the metal-graphene-metal photodetectors, which are commonly fabricated on the doped Si/SiO_2 substrates. In these photodetectors, the incident light is absorbed by the graphene and photoexcited charge carriers are generated. In these photodetectors, the photocurrent is only observed when the light is illuminated to a specific area of the devices such as metal/graphene interface and p-n junction in the channel. Several different photodetection mechanisms, by which the conversion of absorption photons into an electrical signal can be accomplished, has been reported in these photodetectors such as photovoltaic effect,[6,7,15,18] photothermoelectric effect,[8,16,17,23,24] and bolometric effect.[18,21] It has been found that regardless of the photodetection mechanism, the photoresponsivity (photocurrent per unit power of incident light) is relatively low (on the order of mA/W), largely due to the weak light absorption by graphene because monolayer graphene absorbs only 2.3% of the incident light).[6,7,12,13]

Various techniques, such as integrating graphene with photonic nanostructures (e.g., microcavities, waveguides, and plasmonic arrays) have been proposed to increase the photoresponsivity by increasing light absorption.[11,25-28] Using these techniques, the improved responsivity (up to a few tens of mA/W) has been achieved in compared to that observed in the metal-graphene-metal graphene photodetectors. However, the fabrication procedures of the photodetectors by integrating graphene with photonic nanostructures are relatively complex. One previous work showed that the band structure engineering in graphene can also enhance photoresponsivity but only at below room temperatures (< 200 K), while the photoresponsivity at room temperature is still relatively low.[20] It has been also found that hybrid of graphene and other photoactive nanomaterials (such as semiconductor quantum dots) is a promising material for fabricating the photodetectors.[29-31] In this case, photo-carriers are generated in the photoactive materials and then transferred to and transported by graphene, which acts as a conducting channel. Using this approach, the photoresponsivity is increased significantly by the virtue of the much higher photo-absorption by the photoactive nanomaterials but at the expense of more complicated material processing.[29,30]

In this work, we propose and demonstrate another simple photodetection scheme *via* a *field effect mechanism*, which is induced by the interaction of the incident light with an *undoped semiconductor substrate* of a graphene field effect transistor (GFETs) (Fig. 1a). In contrast to the previous graphene photodetectors (commonly fabricated on Si/SiO$_2$ substrates), the undoped silicon carbide (SiC) substrates are also employed as light absorbers in our GFETs. In the presence of the back gate-voltage, the photoexcited carriers in the SiC substrates modulate the electric field, thus also inducing the charge carriers in graphene *via* a field effect. The high sensitivity of the conductivity of graphene to the local change of the electric field provides an efficient intrinsic amplification mechanism that (indirectly) converts the photon energy into a large electrical signal. We validate this field effect based photodetection mechanism with the finite element method (FEM) simulations of the electric and potential field distribution within the GFET for different laser powers (Fig. 1d). We demonstrate that the GFETs fabricated on undoped silicon carbide (SiC) substrates exhibit a high photoresponsivity of ~7.4 A/W at room temperature. The photocurrent and photoresponsivity of the GFETs based on this novel architecture can be tuned by the gate voltage and source-drain bias voltage and is dependent on the incident optical power. The methodology presented here can provide a new and simple pathway for the development of high-responsivity graphene photodetectors (particularly for applications where a high speed of response is not essential).

2. EXPERIMENTAL DETAILS

A typical device architecture of the GFET on an undoped semiconductor substrate (SiC in our case) is shown in Fig. 1a. Monolayer graphene was prepared by a micromechanical exfoliation method from highly ordered pyrolytic graphite (Momentive Performance Materials Inc.) and subsequently transferred (see details of the transfer process in Supplementary Information) onto an undoped 6H (Si-faced) 416 µm thick SiC substrate (Pam-Xiamen, with typical absorption coefficient of ~40 /cm at a wavelength of 400 nm). The source-drain contacts with a channel length of ~2 µm and channel width of ~2 µm were fabricated using electron beam lithography followed by deposition of Cr (5 nm)/Au (65 nm). The back-gate contact was fabricated by deposition of Cr (5 nm)/Au (65 nm) onto the back side of SiC wafer. An optical image (top view) of a part of a fabricated device is displayed in the inset of Fig. 1b. The presence of single-layer graphene is confirmed by Raman spectroscopy (Inset of Fig. 1c, and Supplementary Information). The optoelectronic measurements were performed by illuminating the entire device with a laser beam (wavelength λ = 400 nm, corresponding photon energy = 3.1 eV). The two-terminal dc transport measurements of the GFETs were performed using Keithley 2400 source meters controlled by a LabView program. The photoelectronic response was measured by illuminating the entire device by a laser with a wavelength of 400 nm. The incident laser beam spot size on the device is ~2 mm. The laser power was tuned by controlling the laser drive current and was calibrated using a power meter. All measurements were performed at room temperature and atmospheric pressure.

3. RESULTS

3.1. Substrate-induced field effect photoresponse

Figure 1b shows the measured drain-source current (I_{ds}) as a function of the back-gate voltage (V_g) of a representative device without ("dark") and with laser illumination ("light"). Without illumination, the effect of V_g on the dark current

(I_{dark}) is relatively small. When the device is illuminated, the field effect response is significantly *enhanced*, as demonstrated by a larger gate voltage modulation of the current under laser illumination (I_{light}, Fig. 1b), suggesting that the (same) gate voltage now exerts a stronger electric field on graphene. In Fig. 1c, the photocurrent (I_{photo}, defined as $I_{light} - I_{dark}$) is displayed as a function of V_g. The I_{photo}-V_g plot shows that the photocurrent is positive for sufficiently negative V_g but undergoes a sign reversal near V_g ~0 V and becomes negative for positive V_g. Thus, both the polarity and magnitude of photocurrent of our device can be tuned with the gate voltage.
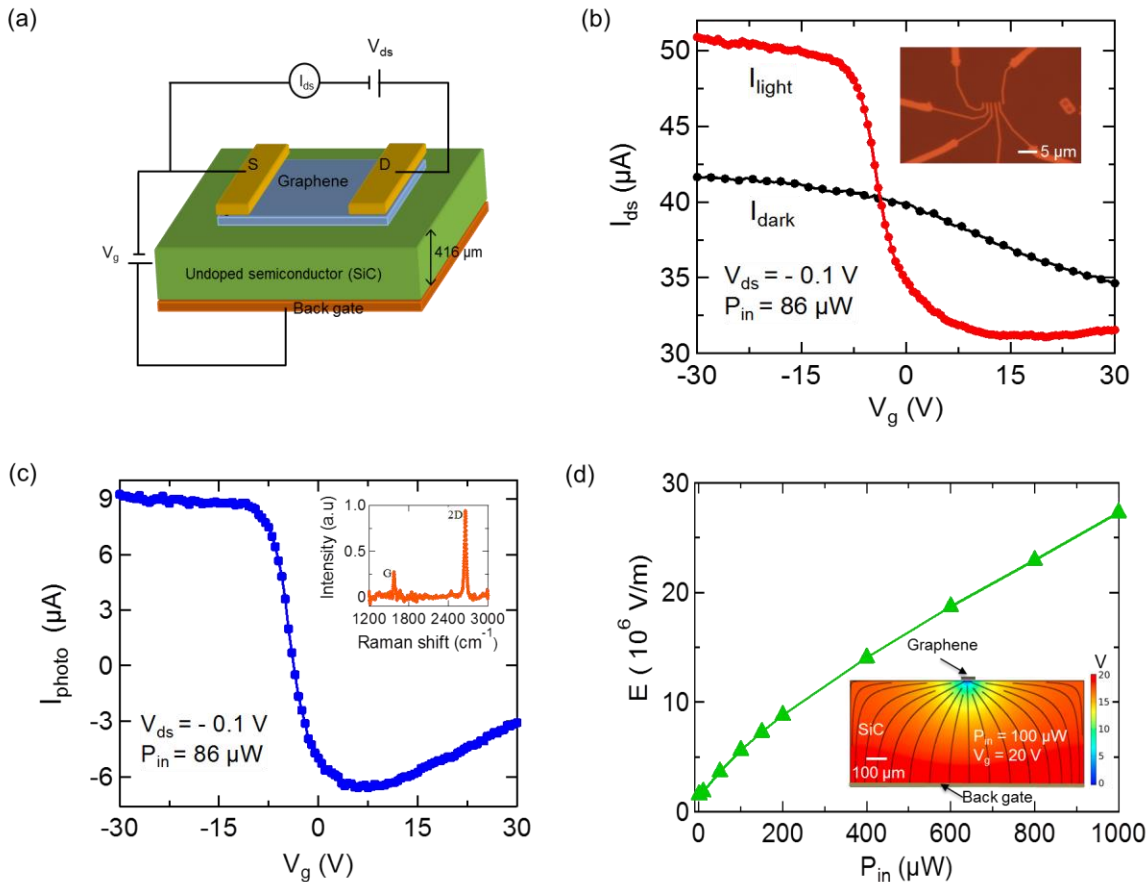

Figure 1. (a) Schematic of a graphene field effect transistor (GFET) on an undoped semiconductor substrate. In this work, an undoped silicon carbide (SiC) is used as the substrate. A back-gate voltage is applied at the back of SiC substrate to produce an electric field acting on the graphene and modulating graphene conductivity *via* field effect. (b) Source-drain current (I_{ds}) as a function of back-gate voltage (V_g) of a GFET on SiC substrate for a fixed $V_{ds} = -0.1$ V, without and with the illumination of a laser (wavelength $\lambda = 400$ nm, laser power incident on device $P_{in} = 86$ μW). Inset: Optical microscope image of a representative GFET device (top view). (c) The dependence of the photocurrent (I_{photo}) of the GFET on gate voltage. The photocurrent is extracted by subtracting the dark current (I_{dark}) from the light current (I_{light}), both shown in Fig. 1b. Inset: Raman spectrum of exfoliated graphene on a SiC substrate, indicating a single layer of graphene. (d) A plot of electric field (E) (simulated with COMSOL Multiphysics) under the graphene as a function of P_{in}, showing an increase in E with increasing incident laser power P_{in}. Inset: A representative simulation of the electric potential (color scale) and electric field lines in a GFET with a back gate voltage (V_g) of 20 V and $P_{in} = 100$ μW. The SiC thickness (416 μm) in the modeled device is the same as the thickness of SiC in our experimental devices. The scale bar for the SiC is 100 μm. The graphene and back-gate electrode are not drawn to the scale. To qualitatively account for the effects of native oxide and spatially non-uniform generation of photo carriers in the substrate, we have assumed the conductivity of the top 10 nm of the SiC to be not affected by illumination. The stream lines represent the electric field lines, which direct the photogenerated carriers toward the location directly under the graphene. The electric field shown in the main panel (d) is calculated at the location under the graphene. The strength of the electric field under graphene increases with increasing P_{in}. The change in the electric field is detected by the change of conductivity of graphene, allowing us to detect the light incident on the GFET.

The observed gate voltage-dependent photocurrent of our GFETs can be qualitatively explained by the following mechanism. Under dark condition, the undoped SiC is highly insulating (bandgap ~3 eV)[32] and the applied V_g drops uniformly across the SiC substrate. Due to the relatively large thickness ($d \sim 416$ μm) of our SiC substrate, the electric field ($E = V_g/d$) experienced by graphene is relatively small, giving rise to a weak field effect. The observed finite small field effect without illumination may arise from the residual conductivity of the SiC due to impurities or trapped charges. When the SiC is illuminated, photo-excited charge carriers are generated in SiC, leading to an increased conductivity. While the SiC becomes more conductive under illumination, the experimentally observed leakage current between the back gate and graphene does not increase notably (the SiC does not form a shorted connection between the backgate and graphene). This can be due to the presence of a native oxide layer that often forms naturally on the SiC surface.[33,34] This native oxide (whose bandgap is much larger than our laser photon energy) remains insulating even under illumination. This could also arise from the spatially non-uniform distribution of the photogenerated carriers in SiC, where parts of the SiC may remain insulating under illumination. The enhanced field effect seen in Fig. 1b suggests that with increasing conductivity of SiC, the electric field at the graphene due to the applied back gate voltage increases. Such a photo-actuated change in the electric field is sensed by the change of graphene conductivity *via* field effect, allowing us to detect the light interacting with SiC.[35] This proposed mechanism is also consistent with the observation of near-zero photocurrent at $V_g \sim 0$ V, where there is no electric field (and thus no field effect) to modulate the graphene conductivity. The small offset of zero crossing point of photocurrent away from $V_g = 0$ V (Fig. 1c) may be related to gate hysteresis and trapped charges in the SiC.[36]

To better understand the field effect based photodetection mechanism, we conducted FEM simulations of the electric field and potential distribution within the SiC substrate in the GFET using COMSOL Multiphysics.[35] The results of our simulation are presented in Fig. 1d. The architecture and thickness of the SiC substrate used in the modeled device closely match that of our experimental devices. To qualitatively capture the effect of the native oxide and the part of SiC substrate that remains insulating under illumination, we assumed the conductivity of the top 10 nm portion of our SiC substrate to be unaffected by illumination in our simulation. The laser illumination modifies the electric field within the SiC *via* the change in conductivity within SiC (except the top 10 nm). The conductivity of SiC affected by illumination is calculated for different incident laser power (see Supplementary Information) and is used as an input to the model which simulates the electric field. A representative result showing the simulated electric potential in the SiC for a laser power of 100 μW is displayed in the inset of Fig. 2d. The calculated electric field under graphene (at the SiC/graphene interface) for various laser powers is plotted in Fig. 2d. The model generally shows that for increasing illumination power a greater electric field exists in the vicinity of graphene (Fig. 1d), which results in the modulation of the conductivity of graphene. This change in graphene conductivity is used to detect the light incident on the GFET.
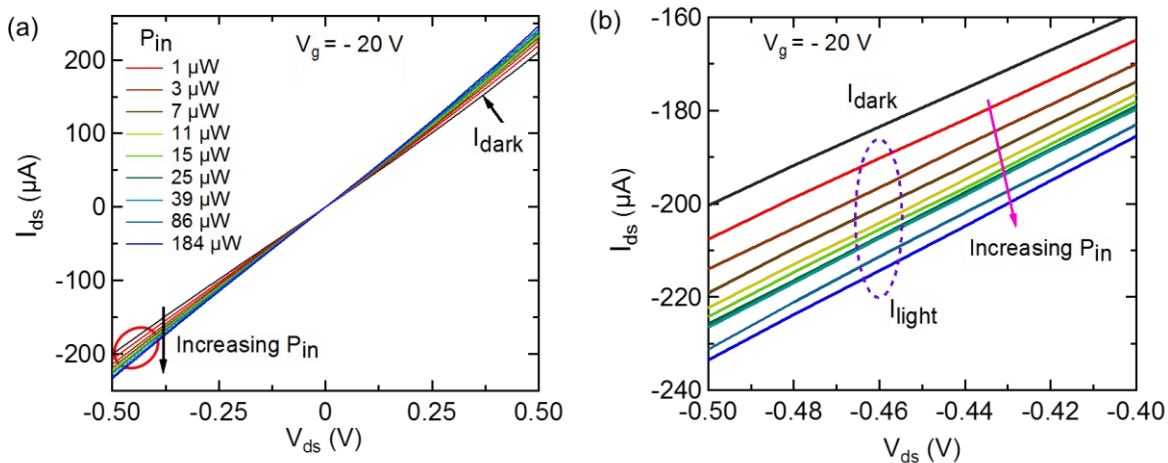

Figure 2. (a) I_{ds} - V_{ds} characteristics of a typical GFET at $V_g = -20$ V without and with illumination for a series of incident laser power P_{in} (varying from 1 to 184 μW). All I_{ds} - V_{ds} curves pass through the origin, while the slope of I_{ds} - V_{ds} curves increase with increasing laser power. (b) An enlarged view of the circled region shown in (a), showing the increase of current (I_{lihgt}) under laser illumination with increasing laser power.

To further validate the proposed mechanism of photoresponse in our GFETs, we fabricated and measured two control devices. One is a SiC device fabricated by making contacts on top of a bare SiC substrate (no graphene in the channel), and another is a dummy device in which gold is used as the channel instead of graphene (see Supplementary Information). Both the control devices show a negligible photocurrent (zero for dummy device, and of order nA for SiC device) and almost no gate-voltage dependent current in the dark and under light illumination at a wavelength of 400 nm. These measurements confirm that the photocurrent of our GFETs does not result from the Schottky contact at the metal/SiC interface or the field effect from the SiC; rather, the photocurrent originates from the modulated charge carriers in the graphene due to graphene field effect. In addition to these control experiments, we also measured the gate leakage current of the GFET, finding that it is small (<1 nA at $V_g = \pm 30$ V), even with light illumination (see Supplementary Information), much lower than the measured photocurrent, which can reach many tens of μA. This further confirms that photocurrent of our GFET is not the result of the collection of charge from the SiC.

3.2. Bias voltage dependence of photoresponse

We further studied the dependence of photoresponse on the source-drain bias voltage (V_{ds}) at different illumination powers. Figure 2a shows the I_{ds}-V_{ds} characteristics of a typical device without and with illumination for a series of incident laser power P_{in} (varying from 1 to 184 μW) for a representative $V_g = -20$ V. We found that all I_{ds} -V_{ds} curves pass through the origin, while the slope (indicating the conductance of graphene) of I_{ds}-V_{ds} curves increase with increasing laser power. Fig. 2b displays an enlarged view of the circled region shown in (a), showing that I_{light} increases with increasing P_{in}. Using the data in Fig. 2a, we calculated the photocurrent (I_{photo}) and plotted its dependence on V_{ds} in Fig. 3a. For all P_{in}, I_{photo} increases linearly with increasing V_{ds}, and a large photocurrent ~34 μA is observed for $V_{ds} = -0.5$ V and $P_{in} = 184$ μW.

One of the most important figures of merit of a photodetector is its photoresponsivity (R), defined as the ratio of photocurrent and the incident laser power, $R = I_{photo}/P_{in}$. The plots of R as a function of V_{ds} at different laser powers (Fig. 3b) show that R increases linearly with increasing V_{ds}, suggesting that the device is in the linear response regime, and the photoresponsivity can be increased by applying a higher V_{ds}. For $V_{ds} = -0.5$ V, our device shows a high photoresponsivity of 7.4 A/W, which is more than three orders of magnitude higher than that previously measured in the ("type-I") graphene photodetectors (with a similar or higher V_{ds}).[7,18,25-28] Notably, the photoresponsivity of our device is not only higher than the photoresponsivity of the conventional GaN UV photodetectors (R ~0.3 A/W)[37] and Si photodetectors (R ~0.5 A/W),[38] but also higher than the required photoresponsivity for most practical applications (~1 A/W)[3,14] we note that the photoresponsivity was calculated using the *total* laser power incident on our entire device, including the area of the substrate that is not covered by graphene. As a result, the photoresponsivity we report here is likely to be underestimated since a part of the laser beam incident on the SiC far away from the graphene may not contribute significantly to the observed photoresponse. We attribute this high photoresponsivity and external quantum efficiency (*EQE*) of our device to the unique device architecture, which supports field effect photodetection mechanism. Unlike the graphene photodetectors reported to date (commonly fabricated on Si/SiO$_2$ substrates and the graphene is used as a light absorber),[6,7,15,18] in our devices the undoped SiC substrate is employed as a light absorber. In the presence of the back-gate voltage, the photoexcited carriers in the SiC modulate the electric field, thus also inducing the charge carriers in graphene via a field effect. The highly sensitive field effect of graphene provides an efficient intrinsic amplification mechanism that (indirectly) converts the photon energy into a large electrical signal and hence leads to a high photoresponsivity. The number of modulated charge carriers (electrons or holes) in the graphene per incident photon (also known as photoconductive gain) in our device can reach as high as ~23 at a laser power of 1 μW (see Supplementary Information). This high photodetection performance combined with the relatively simple device architecture and fabrication process could offer significant advantages in practical applications.
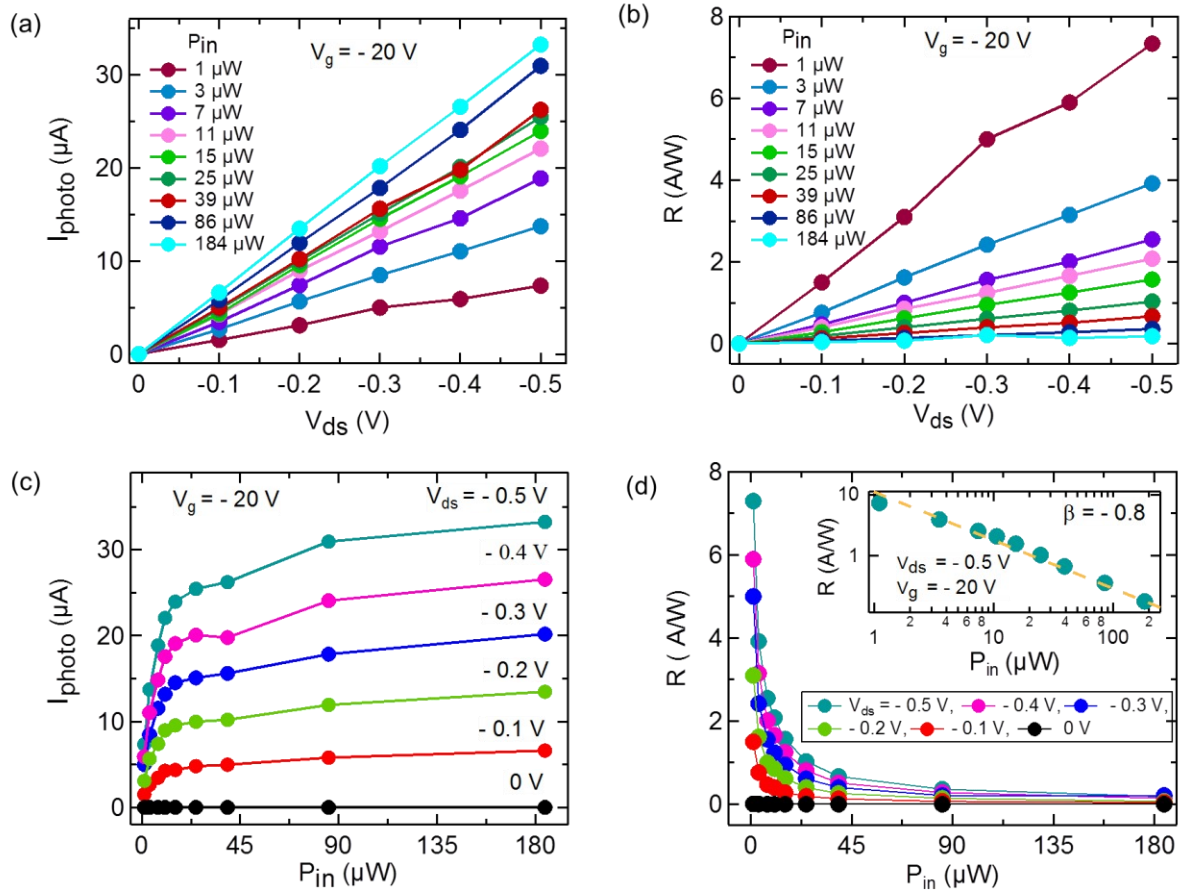
Figure 3. (a) Photocurrent (I_{photo}) at various source-drain bias voltages V_{ds} (from 0 to - 0.5 V) for a series of incident laser powers P_{in} (from 1 to 184 μW) and V_g = - 20 V. (b) Photoresponsivity (R) as a function of V_{ds} for various P_{in} as shown in (a). Both the photocurrent and photoresponsivity increase with increasing V_{ds}. A photoresponsivity of 7.4 A/W is achieved for V_{ds} = - 0.5 V at P_{in} = 1 μW. (c) Photocurrent as a function P_{in} is shown for different V_{ds} (from 0 to - 0.5 V), indicating that photocurrents saturate for higher laser powers for all V_{ds}. (d) The dependence of photoresponsivity on P_{in} for the same V_{ds} as shown in (c). Inset: A log-log plot of R vs. P_{in} for V_{ds} = - 0.5 V. The dashed line is a power law fit ($R \propto P_{in}^{\beta}$) to the experimental data (filled circles) with a power $\beta \sim$ - 0.8.

3.3. Laser power dependent of photoresponsivity

More insight into the photoresponse characteristics of our device can be obtained from the dependence of photocurrent and photoresponsivity on the incident laser power P_{in}. As shown in Fig. 3c, at lower P_{in} (for example, below ~15 μW for V_{ds} = -0.5 V), the photocurrent increases with increasing P_{in} due to an increase in the modulated charge carriers. However, at higher P_{in}, the photocurrent saturates (Fig. 3c), leading to a decrease in the photoresponsivity, as shown in Fig. 3d. One possible reason for this observed photocurrent saturation could be the saturation of graphene field effect itself at large (modulated) charge carrier densities (seen also in Fig. 1b) due to factors such as contact resistance and the existence of charge trap states in graphene or at the graphene-SiC interface. The saturation might also result from decreased electric field modulation in the substrate at higher incident optical powers. We found that the decrease of R with increasing P_{in} can be fitted by a power law, $R \propto P_{in}^{\beta}$ with $\beta \sim$ -0.8 (inset of Fig. 3d). We note that similar power-law relations have been observed in phototransistors based on graphene-MoS$_2$ hybrid with $\beta \sim$ -0.8,[40] and based on black phosphorus with $\beta \sim$ -0.3,[41] (in the latter work this was attributed to the reduction of photogenerated carriers at the higher power due to the recombination/trap states).[41]
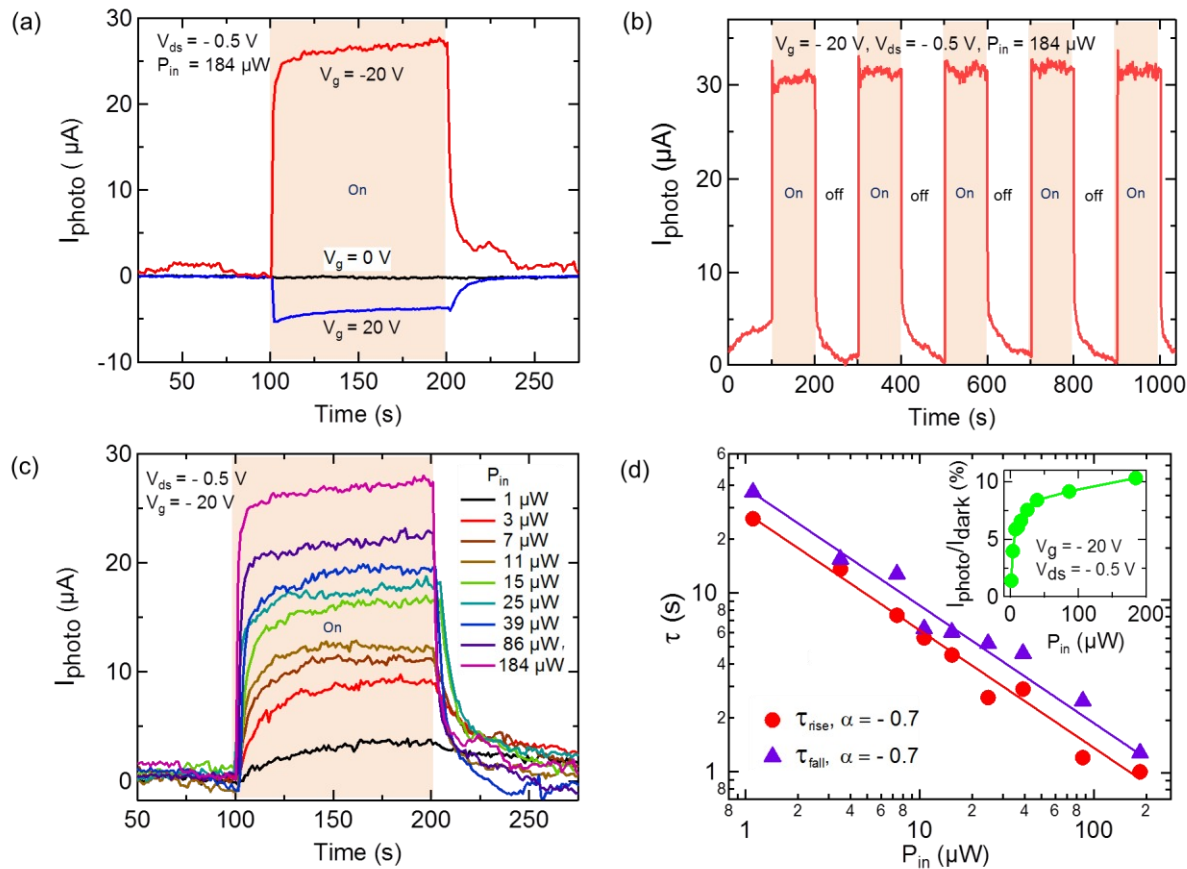
3.4. Photocurrent dynamics

Figure 4. (a) Time-dependent photocurrent of the GFET for V_g of - 20 V, 0 and 20 V, as the laser is turned on and off. A positive photocurrent is observed for V_g = - 20 V, whereas a negative photocurrent is observed for V_g = 20 V. Photocurrent is nearly zero for V_g = 0 V. The sign of the photocurrent is consistent with the field effect measurement in Fig. 1b and c. (b) Time-dependent photocurrent as the laser (P_{in} = 184 μW) is repeatedly turned on and off at V_{ds} = - 0.5 V and V_g = - 20 V. (c) Photocurrent as a function of time at V_{ds} = - 0.5 V, V_g = - 20 V and various incident laser powers P_{in} (from 1 to 184 μW). Shaded regions in (a-c) mark time intervals during which the laser is on. (d) The response time (τ) of the rise and fall of photocurrent dynamics is shown in (c) as a function of P_{in}. The shortest response time of our device is ~ 1 s. Solid straight lines represent power law fits ($\tau \propto P_{in}^{\alpha}$). Inset: The ratio of photocurrent to dark-current I_{photo}/I_{dark} (in %) as a function of P_{in}. The maximum I_{photo}/I_{dark} of our GFET is ~10.5 %, measured for laser power of 184 μW.

We now turn our attention to the transient photoresponse of our devices. Time-dependent photocurrent for different representative gate voltages were measured as the laser was turned on and off (Fig. 4a). It is found that the sign of photocurrent changes from positive to negative as V_g changes from -20 V to +20 V, and the photocurrent is almost zero for V_g = 0 V. Both features are consistent with the field effect measurement shown in the Fig. 1c and confirm the gate tunability of our device's photoresponse. The gate-tunability is important for photodetection since it offers a convenient on-off switching control. In addition to the gate-tunability, our device maintains a long-term stability and a good reproducibility of the photoresponse for a series of repeated laser on/off switching, as shown in Fig. 4b. We found that the characteristics of time-dependent photocurrent curves vary significantly with increasing laser power (Fig. 4c). For a laser power of 184 μW, the photocurrent to dark-current ratio (I_{photo}/I_{dark}) of our device can reach up to 10.3% (inset of Fig. 4d), which is higher than that of other recently reported graphene devices.[42,43] The higher photocurrent to dark-current ratio, long stability, and good reproducibility offer the prospect of robust operation with a good signal-to-noise ratio. We calculated photocurrent response time (τ) by fitting the experimental data in Fig. 4c to an exponential function

(see Supplementary Information) and plotted τ as a function of P_{in} in Fig. 4d. We find that the response time for photocurrent rise (τ_{rise}) and fall (τ_{fall}) for each P_{in} are similar. As the laser power increases, the response time decreases and can be fitted with a power law, $\tau \propto P_{in}^\alpha$, with $\alpha \sim$ -0.7. The shortest response time of our device is ~1 s (measured at the highest P_{in} = 184 µW), which is similar to the response time of a graphene-quantum dot hybrid photodetector.[30] Since the response time is relatively long, our devices can be used for lower temporal bandwidth, such as video imaging applications.[39] We note that the response time of our GFET is much longer than the carrier lifetime in SiC, and is dependent on many factors including the magnitude of the change in electric field, RC time constant of the device, and electrochemical effects.[36] A longer carrier lifetime in SiC may increase the speed of GFET (reduce the device response time) because of the increased accumulation of steady state charge carriers, which increases the SiC conductivity and increases the electric field and the photocurrent response. Indeed, we have observed that the device response time is shorter at larger photocurrent response.

4. CONCLUSIONS

We have demonstrated a novel and relatively simple approach to photodetection with a high photoresponsivity using a graphene phototransistor fabricated on an undoped SiC substrate. The photoresponse characteristics of the device based on this new architecture show many distinct advantages, including high photoresponsivity at room temperature and simple device fabrication process. The high photoresponsivity (~7.4 A/W) of our device is not only superior to most other recently developed graphene photodetectors but also higher than the required photoresponsivity (1 A/W) in most practical applications. We anticipate that the photoresponsivity of devices based on the demonstrated approach can be further improved by optimizing the fabrication processes and measurement conditions (e.g., increasing source-drain bias voltage). In addition, our devices also demonstrate high photoconductive gain, high photocurrent-to-dark-current ratio, and good reproducibility. Moreover, our method may take advantage of a wide range of undoped semiconductors (differing in bandgaps and other electro-optical properties) as substrates for fabricating photodetectors. Recently we have demonstrated that our devices can be used for nonlocal, position-sensitive, and large-area photodetection.[44] Our simple approach can also be generalized to other "beyond-graphene" 2D-semiconductors such as molybdenum disulfide (MoS_2),[45] or to higher-energy radiation.[35] Given the significant design flexibility and simplicity of our approach, this work provides a promising groundwork for the future development of graphene-based high-performance optoelectronic devices.

ACKNOWLEDGEMENTS

AUTHOR CONTRIBUTIONS

B.K.S. fabricated the devices, performed the experiment and analyzed the data, with advice from Y.P.C. I.C. participated in the experiment. E.C. and I. J. contributed to the interpretation of the results. All authors contributed to writing of the manuscript.

SUPPLEMENTARY INFORMATION

Experimental details, Raman characterization, control experiments, leakage current measurement, modulated charge carriers, and time constant analysis are discussed in Supplementary Information.

REFERENCES

[1]   Geim, A. K. and Novoselov, K. S. "The rise of graphene," Nature Mater. 6, 183-191 (2007).

[2]   Geim, A. K. "Graphene: Status and prospects," Science 324, 1530-1534 (2009).

[3]   Novoselov, K. S. *et al.* "A roadmap for graphene," Nature 490, 192-200 (2012).

[4]   Bonaccorso, F., Sun, Z., Hasan, T. and Ferrari, A. C. "Graphene photonics and optoelectronics," Nature Photon. 4, 611-622 (2010).

[5]   Avouris, P. and Xia, F. "Graphene applications in electronics and photonics," MRS Bull. 37, 1225-1234 (2012).

[6]   Xia, F. N., Mueller, T., Lin, Y. M., Valdes-Garcia, A. and Avouris, P. "Ultrafast graphene photodetector," Nature Nanotechnol. 4, 839-843 (2009).

[7]   Mueller, T., Xia, F. N. A. and Avouris, P. "Graphene photodetectors for high-speed optical communications," Nature Photon. 4, 297-301 (2010).

[8]   Gabor, N. M. *et al.* "Hot carrier-assisted intrinsic photoresponse in graphene," Science 334, 648-652 (2011).

[9]   Vicarelli, L. *et al.* "Graphene field-effect transistors as room-temperature terahertz detectors," Nature Mater. 11, 865-871 (2012).

[10] An, X., Liu, F., Jung, Y. J. and Kar, S. "Tunable graphene–silicon heterojunctions for ultrasensitive photodetection," Nano Lett. 13, 909-916 (2013).

[11] Pospischil, A. *et al.* "CMOS-compatible graphene photodetector covering all optical communication bands," Nature Photon. 7, 892-896 (2013).

[12] Li, J., Niu, L., Zheng, Z. and Yan, F. "Photosensitive graphene transistors," Adv. Mater. 26, 5239–5273 (2014).

[13] Sun, Z. and Chang, H. "Graphene and graphene-like two-dimensional materials in photodetection: mechanisms and methodology," ACS Nano 8, 4133-4156 (2014).

[14] Liu, C.-H., Chang, Y.-C., Norris, T. B. and Zhong, Z. "Graphene photodetectors with ultra-broadband and high responsivity at room temperature," Nature Nanotechnol. 9, 273-278 (2014).

[15] Xia, F. N. *et al.* "Photocurrent imaging and efficient photon detection in a graphene transistor," Nano Lett. 9, 1039-1044 (2009).

[16] Shi, Y., Fang, W., Zhang, K., Zhang, W. and Li, L. J. "Photoelectrical response in single-layer graphene transistors," Small 5, 2005-2011 (2009).

[17] Xu, X., Gabor, N. M., Alden, J. S., van der Zande, A. M. and McEuen, P. L. "Photo-thermoelectric effect at a graphene interface junction," Nano Lett. 10, 562-566 (2010).

[18] Freitag, M., Low, T., Xia, F. N. and Avouris, P. "Photoconductivity of biased graphene," Nature Photon. 7, 53-59 (2013).

[19] Freitag, M., Low, T. and Avouris, P. "Increased responsivity of suspended graphene photodetectors," Nano Lett. 13, 1644-1648 (2013).

[20] Zhang, Y. Z. *et al.* "Broadband high photoresponse from pure monolayer graphene photodetector," Nature Commun. 4, 1811 (2013).

[21] Kim, M. H. *et al.* "Photothermal response in dual-gated bilayer graphene," Phys. Rev. Lett. 110, 247402 (2013).

[22] Withers, F., Bointon, T. H., Craciun, M. F. and Russo, S. "All-graphene photodetectors," ACS Nano 7, 5052-5057 (2013).

[23] Herring, P. K. *et al.* "Photoresponse of an electrically tunable ambipolar graphene infrared thermocouple," Nano Lett. 14, 901-907 (2014).

[24] Echtermeyer, T. J. *et al.* "Photothermoelectric and photoelectric contributions to light detection in metal–graphene–metal photodetectors," Nano Lett. 14, 733–3742 (2014).

[25] Liu, Y. *et al.* "Plasmon resonance enhanced multicolour photodetection by graphene," Nature Commun. 2, 579 (2011).

[26] Furchi, M. *et al.* "Microcavity-integrated graphene photodetector," Nano Lett. 12, 2773-2777 (2012).

[27] Gan, X. *et al.* "Chip-integrated ultrafast graphene photodetector with high responsivity," Nature Photon. 7, 883-887 (2013).

[28] Wang, X. M., Cheng, Z. Z., Xu, K., Tsang, H. K. and Xu, J. B. "High-responsivity graphene/silicon-heterostructure waveguide photodetectors," Nature Photon. 7, 888-891 (2013).

[29] Konstantatos, G. *et al.* "Hybrid graphene-quantum dot phototransistors with ultrahigh gain," Nature Nanotechnol. 7, 363-368 (2012).

[30] Sun, Z. *et al.* "Infrared photodetectors based on CVD-grown graphene and PbS quantum dots with ultrahigh responsivity," Adv. Mater. 24, 5878-5883 (2012).

[31] Huang, Y. Q., Zhu, R. J., Kang, N., Du, J. and Xu, H. Q. "Photoelectrical response of hybrid graphene-PbS quantum dot devices," Appl. Phys. Lett. 103, 143119 (2013).

[32] Persson, C. and Lindefelt, U. "Relativistic band structure calculation of cubic and hexagonal SiC polytypes," J. Appl. Phys. 82, 5496-5508 (1997).

[33] Da Silva, C. R. S., Justo, J. F. and Pereyra, I. "Crystalline silicon oxycarbide: Is there a native oxide for silicon carbide?," Appl. Phys. Lett. 84, 4845-4847 (2004).

[34] Amy, F., Soukiassian, P., Hwu, Y. and Brylinski, C. "Si-rich 6H-and 4H-SiC (0001) 3×3 surface oxidation and initial SiO_2/SiC interface formation from 25 to 650°C," Phys. Rev. B 65, 165323 (2002).

[35] Foxe, M. *et al.* "Graphene field-effect transistors on undoped semiconductor substrates for radiation detection," Nanotechnology, IEEE Trans. 11, 581-587 (2012).

[36] Cazalas, E. *et al.* "Hysteretic response of chemical vapor deposition graphene field effect transistors on SiC substrates," Appl. Phys. Lett. 103, 053123 (2013).

[37] Butun, B., Tut, T., Ulker, E., Yelboga, T. and Ozbay, E. "High-performance visible-blind GaN-based p-i-n photodetectors," Appl. Phys. Lett. 92, 033507 (2008).

[38] Kim, C. O. *et al.* "High photoresponsivity in an all-graphene p–n vertical junction photodetector," Nature Commun. 5, 4249 (2014).

[39] Koppens, F. H. L. *et al.* "Photodetectors based on graphene, other two-dimensional materials and hybrid systems," Nature Nanotechnol. 9, 780-793 (2014).

[40] Xu, H. *et al.* "High responsivity and gate tunable graphene-MoS_2 hybrid phototransistor," Small 10, 2300-2306 (2014).

[41] Buscema, M. *et al.* "Fast and broadband photoresponse of few-layer black phosphorus field-effect transistors," Nano Lett. 14, 3347-3352 (2014).

[42] Roy, K. *et al.* "Graphene-MoS_2 hybrid structures for multifunctional photoresponsive memory devices," Nature Nanotechnol. 8, 826-830 (2013).

[43] Liu, N. *et al.* "Large-area, transparent, and flexible infrared photodetector fabricated using p-n junctions formed by n-doping chemical vapor deposition grown graphene," Nano Lett. 14, 3702-3708 (2014).

[44] Biddut K. Sarker, Edward Cazalas, Ting-Fung Chung, Isaac Childres, Igor Jovanovic, and Yong P. Chen, "Position dependent and millimeter-range photodetection in phototransistors with micron-scale graphene on SiC," Nature Nanotechnol. 12, 668-674 (2017).

[45] Lopez-Sanchez, O., Lembke, D., Kayci, M., Radenovic, A. and Kis, A. "Ultrasensitive photodetectors based on monolayer MoS_2," Nature Nanotechnol. 8, 497-501 (2013).

Supplementary Information

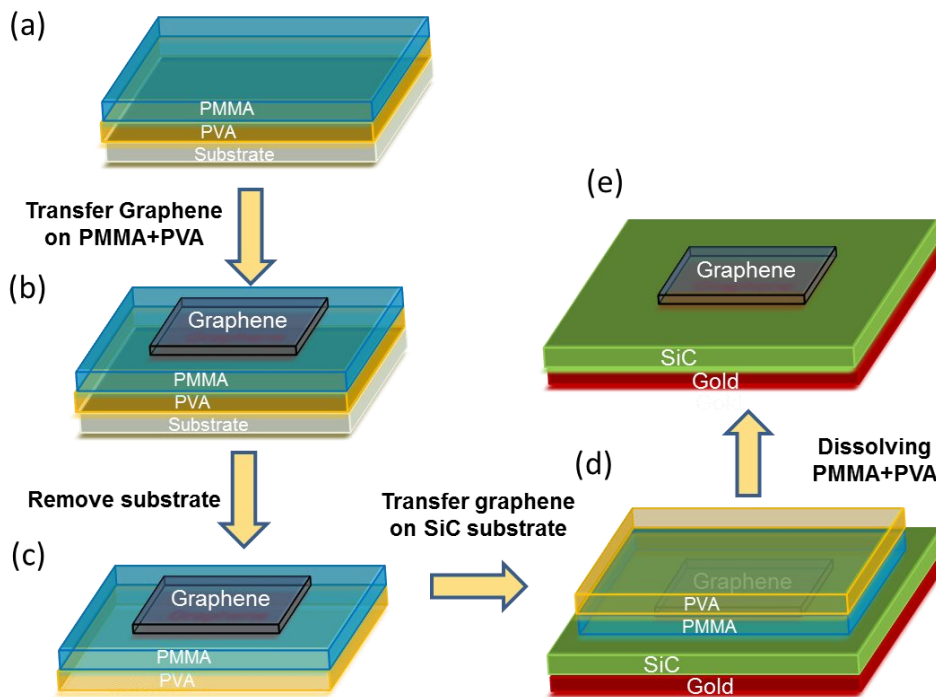## 1. Transfer of the exfoliated graphene onto SiC substrate

Figure S1. Schematic of the process to transfer an exfoliated monolayer graphene onto a SiC substrate.

We transfer an exfoliated monolayer graphene onto a silicon carbide (SiC) substrate by the following processes. First, polyvinyl alcohol (PVA) solution is coated on a sacrificial substrate (here, Si/SiO$_2$ with a dimension of 2×2 cm is used) at 3000 rpm for 45 s and baked on a hotplate at 90 $^\circ$C for 5 min. Then PMMA (polymethyl methacrylate) is coated onto the PVA film and similarly baked (Fig. S1a). Monolayer graphene was prepared by the micromechanical exfoliation technique and transferred onto the polymer (PVA/PMMA) films (Fig. S1b). The polymer film containing the graphene is then separated from the sacrificial substrate (Fig. S1 c) and transferred onto an undoped SiC substrate using a homemade transfer stage (Fig. S1d). Finally, the SiC substrate is submerged in acetone for a few hours to remove the polymer films (PVA/PMMA), then rinsed with IPA (isopropyl alcohol) and blown dry with nitrogen gas (Fig. S1e).

2. Raman characterization of the graphene on SiC substrate

We used Raman spectroscopy to confirm that the transferred exfoliated graphene on the SiC substrate is a monolayer. The Raman spectrum is measured using a Horiba Jobin Yvon Xplora confocal Raman microscope with a 532 nm excitation laser. Spectra were taken under the same experimental conditions on the same device at two different spots; one spot is on the graphene on the SiC substrate, and the other spot is on the SiC substrate (where no graphene is present) (inset in Fig. S2b). Since the intensity of Raman peaks varies slightly from spot to spot, the spectra were normalized by the strongest peaks. Since the Raman spectra of graphene and SiC have substantial overlap with each other, we subtracted the normalized SiC spectrum (Fig. S2a) from the normalized spectrum of graphene on the SiC (graphene + SiC) (Fig. S2b).

The difference of the normalized spectrum of SiC, and graphene on the SiC is the graphene spectrum, which is shown in the inset of Fig. 1c in the main text. The graphene spectrum shows no detectable D peak, suggesting negligible defects in graphene.[1] The ratio of the 2D to G peaks intensity (I_{2D}/I_G) of the graphene spectrum is more than two, indicating a monolayer graphene in our device (inset, Fig. 1c).[1,2]
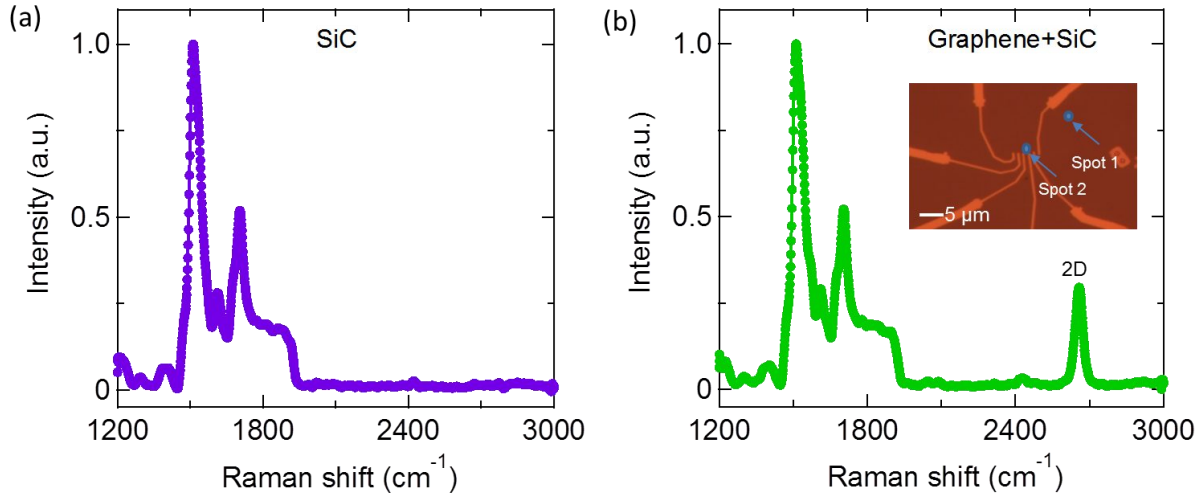

Figure S2. Raman spectrum of (a) SiC substrate (without graphene) and (b) graphene on SiC. Inset of (b): Optical image of a fabricated device. Spots 1 (SiC) and 2 (graphene on SiC) show where the Raman spectra were taken. The spectrum intensity is normalized by its strongest peak (near 1500 cm^{-1}). The difference between the spectra (b) and (a) is extracted as the graphene Raman spectrum and shown in the inset of Fig. 1c.

3. SiC conductivity

The conductivity of the SiC substrate increases by absorption of the incident light, whereby electrons and holes are produced in the SiC. The change in SiC conductivity due to light illumination can be calculated by $\Delta\sigma = q\mu = q'\tau\mu$, where $q(=q'\tau)$ is the number of steady state carriers produced per unit volume and q' is the number of carriers produced per unit volume per unit time through light absorption, μ is the sum of electron and hole mobility (490 cm^2/V·s, given by manufacturer, PAM-Xiamen) of the carriers within SiC and τ is the carrier life time (recombination time), the mean time a conductive charge may exist within the substrate before recombination with an opposite charge.

Here we assume that $\tau = 1$ μs [Ref. 3,4]. We note that a longer carrier lifetime (even though the carrier lifetime is a fixed quantity for our SiC and not tunable in our experiment) would increase steady-state photogenerated charge carriers and lead to higher photocurrent response (similar to the effects of increasing photo power). We consider the influence of penetration depth of the light in the SiC substrate. For simplicity, we divided the total thickness of SiC substrate into three parts and the profile of light absorption throughout the depth of the SiC substrate is used to calculate charge density produced per unit time for each part. For example, the time-dependent number of carrier change per unit volume for the top 1/3 of SiC substrate is calculated to be $q' = 1.04\times10^3$ C/m^3/s for $P_{in} = 1$ μW. The final SiC conductivity of the top 1/3 SiC substrate due to laser irradiation is given as $\sigma = \sigma_t + \Delta\sigma = 1\times10^{-3} + P_{in}(4.2\times10^{-5})$ S/m, where P_{in} is in μW and σ_t is typical value of un-irradiated SiC conductivity, $\sigma_t \approx 1\times10^{-3}$ S/m is given the manufacturer (PAM-Xiamen).

4. Gate leakage current of device in dark and under laser illumination

To confirm that gate leakage current (I_g) is not contributing to the photocurrent of our device, I_g is monitored in both the dark and light illumination conditions. Figure S3a, b and c show the plots of I_g as a function of gate-voltage (V_g), I_g as a function of source-drain bias (V_{ds}), and I_g as a function of time, respectively, measured in the dark and under illumination with various incident laser powers (P_{in}) on the device.
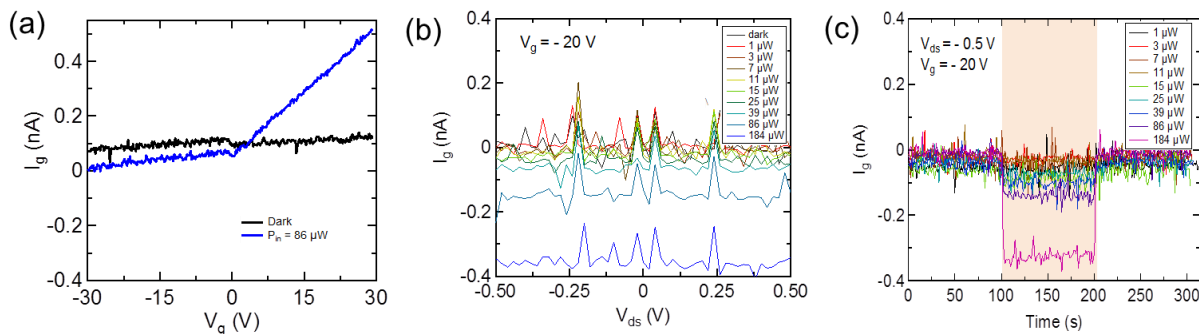
Figure S3. (a) Gate leakage current (I_g) *vs.* gate voltage (V_g), (b) I_g *vs.* source-drain bias voltage (V_{ds}), (c) I_g *vs.* time, measured in the dark and under illumination with various incident laser powers (P_{in}) ranging from 1 to 184 µW. The shaded region in (c) labels the time interval when the laser is turned on.

From these plots (Fig. S3a-c), we found that the device (i) leakage current is small (<1 nA) compared to the measured photocurrent (in the range of µA), and that (ii) leakage currents both in the dark and under laser illumination with a low laser power are almost similar. These features indicate that leakage current does not increase significantly with a low incident laser power. While the leakage current does increase for a higher laser power, it remains less than 1 nA. We, therefore, conclude that gate leakage current does not contribute to the measured photocurrent in our device.

5. Control experiment 1: SiC device (without graphene)

To confirm the photoresponse of our GFETs is not due to the photoresponse of the substrate (SiC) or Schottky contact at the SiC/metal interface, we fabricated SiC control devices without graphene (making a direct contact on top of SiC). Optical image of a fabricated SiC device (without graphene) is shown in the inset of Fig. S4a. The plots of I_{ds}-V_g and I_{photo}-V_g characteristics of a representative SiC device with and without illumination are shown in Fig. S4a,b, respectively. We use the same scale in the Figs. S4b and 1c (I_{photo}-V_g of GFET in the main figure) in order to clearly show the difference between the photocurrents and their gate dependence in the GFET and SiC devices.
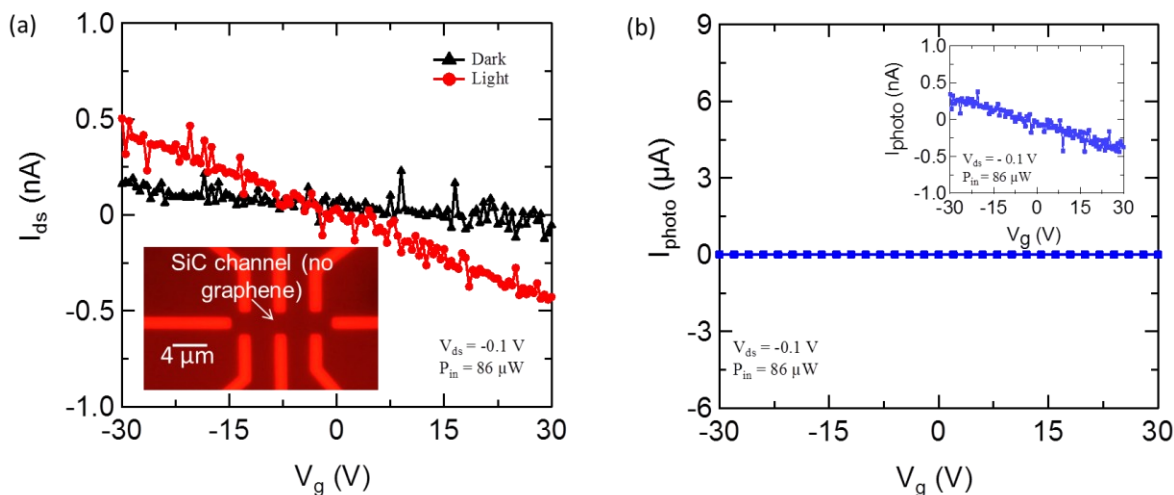

Figure S4. (a) Dependence of the drain-source current on the back-gate voltage (I_{ds} – V_g) of a SiC device (without graphene) without and with laser illumination (λ = 400 nm) at an incident laser power (P_{in}) of 86 µW. Inset: Optical image of a fabricated SiC device (without graphene). (b) The dependence of the photocurrent (I_{photo}) of the GFET on the gate voltage.

The scales of Figs.4Sb and 1c (in the main text) are kept the same to clearly show the differences in the gate dependence of photocurrent generation. Inset: the same Fig.4Sb plot, but on a nA scale.

These plots show that both the current (in dark as well as under illumination) and photocurrent of SiC device are very small (of the order nA), at least three orders lower than that observed photocurrent in the GFET (of the order µA). In addition, the photocurrent in the SiC device does not change significantly with the gate voltage, whereas the photocurrent in GFETs shows strong gate-voltage dependence (Fig. 1c). From those measurements we can conclude that the photoresponse of our GFETs does not result from the Schottky contact of SiC or the collection of the charge from the SiC; rather it is the result of the modulation of charge carriers in the graphene via field effect.

6. Control experiment 2: Dummy device (gold in the channel instead of graphene)

We also fabricated dummy devices that contain no graphene, but use gold as a channel between the source-drain contacts (Inset of Fig. S5a). The I_{ds} - V_g plot of the dummy device shows no change in source-drain currents with the gate-voltage, with and without illumination. The I_{ds} - t characteristics also show no change in current under light illumination (Fig. S5b). These observations further confirm that graphene is essential for the field effect photoresponse observed in the GFETs, and the photoresponse does not come from the SiC substrate or SiC-Au interface.
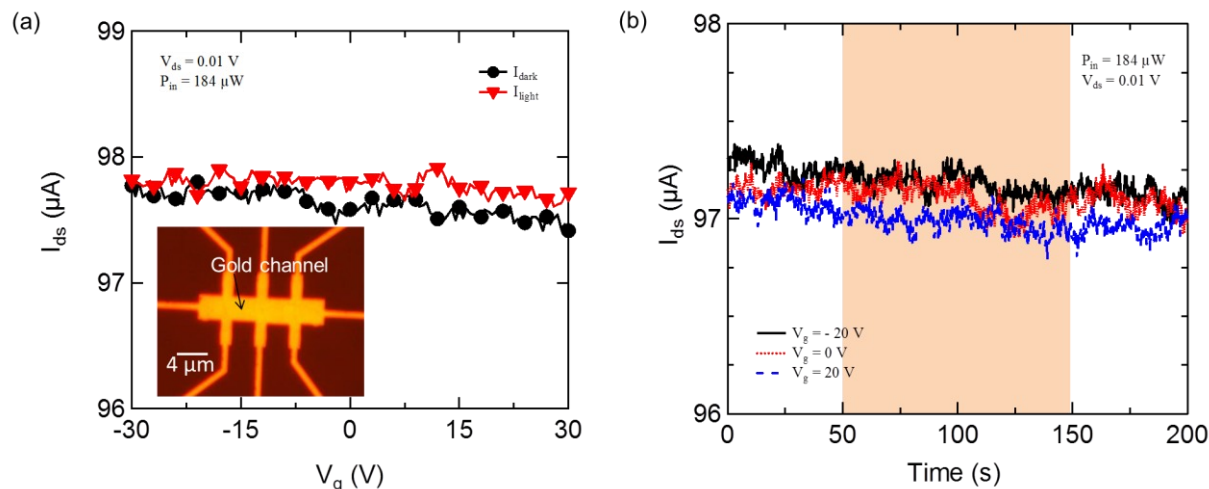

Figure S5. (a) I_{ds} - V_g characteristics of a dummy device without and with laser illumination (λ = 400 nm). Inset: Optical image of a fabricated dummy device (gold in the channel instead of graphene) (b) I_{ds} - t characteristics for different the gate voltages when the laser switches on and off. Shaded area indicates the time intervals during which the laser is on.

7. Modulated charge carriers per incident photon

The number of modulated charge carriers in the device per incident photon is calculated using the formula,[5] $(I_{photo}/P_{in}) \times (hc/e\lambda)$, where I_{photo} is the photocurrent, P_{in} is the incident laser power on the device, h is Planck's constant, e is electron charge, and λ is the wavelength of incident light (400 nm). The number of modulated charge carriers per incident photon increases with increasing source-drain bias voltage because photocurrent increases with increasing the source-drain bias. We found that for a source-drain bias of -0.5 V, approximately 23 electrons (or holes) can be modulated in graphene by a single photon incident into the SiC substrate of our device.

8. Photocurrent response time

The photocurrent (I_{photo}) rise and fall response times (τ) for all laser powers were calculated by fitting the photocurrent $vs.$ time data to an exponential function. Four representative fitted curves (for both rise and fall) for two different laser

powers of 184 µW and 25 µW are shown in Fig. S6. The rise and fall times for P_{in} = 184 µW are found to be 1.0 and 1.3 s, respectively, whereas for P_{in} = 25 µW, the rise and fall time are 2.6 and 5.6 s, respectively.
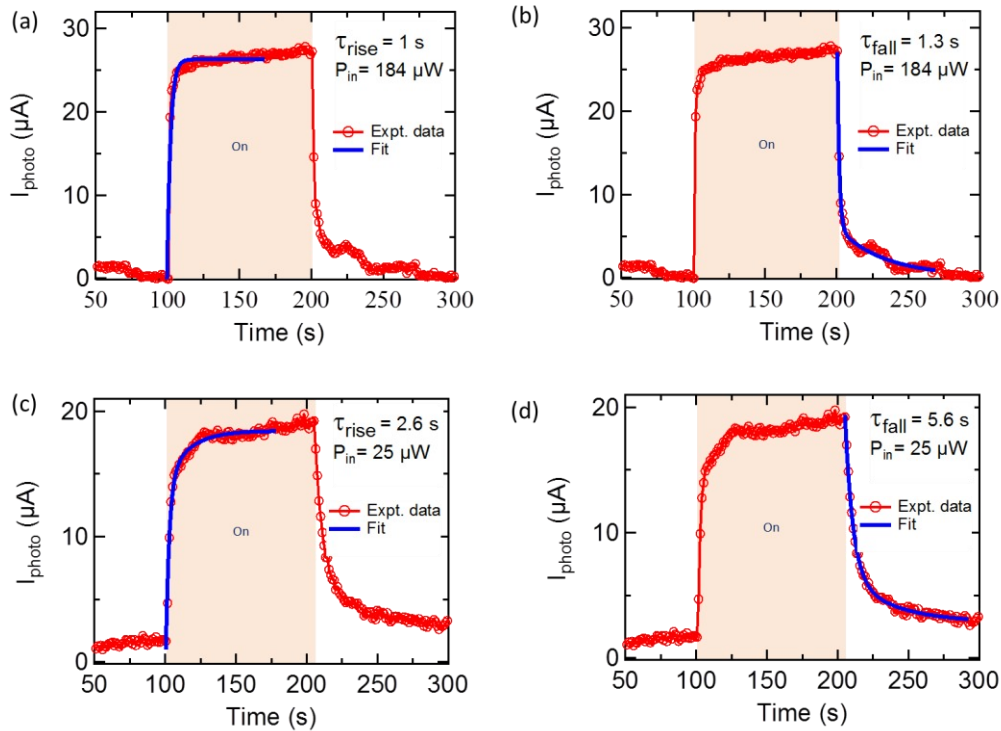

Figure S6. (a-d) Photocurrent (I_{photo}) *vs.* time for V_g = - 20 V and V_{ds} = - 0.5 V (a, b) for incident laser powers (P_{in}) of 184 µW and (c, d) P_{in} = 25 µW. Red circles are experimental data; solid lines represent exponential fits to extract the time constants. Shaded regions in a-d label time intervals during which the laser is on.

Supplementary references

[1] Cançado, L. G. *et al.,* "Quantifying defects in graphene via Raman spectroscopy at different excitation energies," Nano Lett. 11, 3190-3196 (2011).
[2] Ferrari, A. C. *et al.*, "Raman spectrum of graphene and graphene layers," Phys. Rev. Lett. 97, 187401 (2006).
[3] Galeckas, A., Linnros, J., Frischholz, M. and Grivickas, V., "Optical characterization of excess carrier lifetime and surface recombination in 4H/6H–SiC," Appl. Phys. Lett. 79, 365-367 (2001).
[4] Kordina, O., Bergman, J. P., Henry, A. and Janzén, E., "Long minority carrier lifetimes in 6H SiC grown by chemical vapor deposition," Appl. Phys. Lett. 66, 189-191 (1995).
[5] Prins, F. *et al.,* "Fast and efficient photodetection in nanoscale quantum-dot junctions," Nano Lett. 12, 5740-5743 (2012).